JOM, Vol. 68, No. 12, 2016
DOI: 10.1007/s11837-016-2123-7

Mechanical Properties and Microstructural Evolution of Bimetal 1050/Al_2O_3/5083 Composites Fabricated by Warm Accumulative Roll Bonding

M. SEDIGHI,[1,3] P. FARHADIPOUR,[1] and M. HEYDARI VINI[2]

1.—School of Mechanical Engineering, Iran University of Science and Technology, Tehran 16844, Iran. 2.—Department of Mechanical and Aerospace Engineering, Science and Research Branch, Islamic Azad University, Tehran, Iran. 3.—e-mail: sedighi@iust.ac.ir

In this study, a warm accumulative roll bonding process was used to produce a 1050/5% Al_2O_3/5083 composite from AA1050 and AA5083 sheets. Firstly, the raw materials were roll-bonded and then rolled up to five accumulative rolling cycles by preheating for 5 min at 280°C before each cycle. The mechanical properties of the ARBed bimetals were evaluated in comparison with 1050/5% Al_2O_3 and 5083/5% Al_2O_3 roll-bonded single-metal metal matrix composites (MMCs). It was found that two different layers of the bimetal sheet (1050/5% Al_2O_3/5083 composite) were deformed in a nearly identical way during the first three cycles. After that, the 5083 layers started necking. The strength of the bimetal samples was superior to the average of these two single-metal MMCs. Furthermore, the strength and ductility of the ARBed bimetal improved by ARB cycles. Finally, the fracture surfaces of the bimetal composite were studied at all ARB cycles by scanning electron microscopy.

INTRODUCTION

Nowadays, a growing need is felt for the use of bimetal composites with special capabilities and characteristics, including light weight, higher mechanical properties, corrosion resistance and good wear and thermal stability. Bimetallic aluminum alloys have become increasingly popular for engineering applications, since they usually possess several desirable properties. They are applied in various fields such as the aerospace, automotive, vessel, and electrical industries.[1,2] Severe plastic deformation (SPD) techniques are employed to fabricate metal matrix composites (MMCs), namely powder metallurgy (PM),[3] squeeze casting and spray forming,[4,5] accumulative roll bonding (ARB),[6] equal channel angular pressing (ECAP), cyclic extrusion compression (CEC), and multi-axial forging (MAF). These processes are utilized to produce ultrafine-grain (UFG) materials.[7] The ARB process was first proposed by Saito et al.[7] During this process, two layers are rolled after preparation and stacked together. Generally, the thickness reduction per each cycle of rolling is 50%, and the two sheets are bonded together. The ARB process of each cycle is conducted in several steps, including cutting, surface degreasing with acetone, brushing, stacking together, and rolling. In this regard, different kinds of bimetal materials such as Al/Mg,[8–11] Al/Cu,[12] Al/Ni, Al/Ti[1] and Al/Zn[14] can be mentioned.

Researchers have found that at the initial cycles of a bimetal ARB process, both materials deform in a similar way.[13–15] They have illustrated that, by increasing the number of ARB cycles, plastic instabilities in the harder material layers occur earlier, and the harder material involves necking and fracture. This deformation behavior causes the homogeneously distributed fragmentation of the hard material in the soft material matrix. The necking and rupture of the hard layers influence the mechanical properties of the composite. Some works have reported that, despite the fracture of the hard layers, the strength of the composite increases.[13–15] Some research has been conducted to investigate the process with two different grades from the same base metals such as Al/Al(Sc),[16] AA1050/AA5754,[17] AA6014/AA5754,[17] AA2219/AA5086,[18] and AA1050/AA6061.[19] Moreover, ceramic particles like SiC, TiC, WC, SiO_2, ZrO_2, and B_4C are employed as reinforcement particles in MMCs with similar metal laminates.[20–22]

(Published online October 5, 2016)

The aim of the present study is to fabricate bimetal particle-reinforcing MMCs via warm accumulative roll bonding (warm-ARB) with higher toughness. First, the material prepration and manufacturing process are explained. Then, the microstructure and mechanical properties of the composites such as strength, fracture surface, elongation, and toughness of the fabricated 1050/Al_2O_3/5083 composites are investigated.

MATERIALS AND EXPERIMENT

Materials

In the present study, two different commercial aluminum alloys, namely AA1050 and AA5083, have been used for warm-ARB processing. The detailed chemical compositions of these alloys are given in Table I.

Warm-ARB Processing

Initially, the Al strips were annealed at 400°C for 1 h. Subsequently, 1050 and 5083 strip samples of 200 × 50 × 2 mm were degreased in an acetone bath and scratch-brushed with a stainless steel circumferential brush in order to remove the oxide layer from the surfaces. Each of the 1050 and 5083 strips was stacked together to obtain 4 mm thickness, while alumina particles with average particle size of 2 μm were dispersed among them by 5 vol.% fraction. The stacked strips were fastened by wires at both ends to secure proper alignment of the two strips. Then, they were roll-bonded to 1 mm thickness (75% reduction equal to effective strain of 1.6) at 400°C without any lubrication (Fig. 1a). A rolling machine with roll diameter of 170 mm, rotational speed of 36 rpm, and a power capacity of 35 hp was utilized. After the first rolling cycle, MMC strips containing Al_2O_3 particles (between 1050 and 5083 layers) were fabricated. Hereafter, this sample is called the primary composite or cycle#0 (Fig. 1a) in this paper. To remove the work hardening effects of the cycle#0 of the ARB process, the primary composite was annealed at 400°C for another 1 h.

Higher rolling temperature and thickness reduction increase the bond strength of the composite layers.[23] For this reason, the reduction percentage of the first cycle is more than the others. In the present study, the thickness reduction in the zero cycle (cycle#0) is 75% (effective von Mises strain of 1.6) and in the other cycles is 50% (effective von Mises strain of 0.8).

In the next step (Fig. 1b), the composite was cut into two strips by a cutting machine. The two strips of MMC were stacked together after degreasing and wire-brushing to obtain 2 mm thickness. They were then roll-bonded by 50% reduction after heating at 280°C for 5 min. It has been reported that the thickness of the oxide film on cold rolled aluminum strip is about 2.5–2.8 nm, while the oxide film thickness of the strips annealed at 280–300°C for 20–30 h is about 4 nm.[24] Therefore, the size of native oxide layers of the contacting 1050 and 5083 layers during roll bonding is negligible in comparison with the average size of alumina particles (2 μm). The warm-ARB process was repeated for another five cycles. During these five warm-ARB cycles, it is expected that the Al_2O_3 particles are dispersed more and more homogeneously. The steps of the production process of the 1050/Al_2O_3/5083 composite are summarized in Table II.

The tensile test specimens were machined from the rolled strips according to the ASTM E8M standard,[25] which were oriented along the longitudinal direction. The gauge length and the width of the tensile test specimens were 25 mm and 6 mm, respectively. The tensile tests were conducted at ambient temperature on a H50KS testing machine at a strain rate of 1.67×10^{-4} S^{-1}. For each sample, the tensile test was repeated three times.

RESULTS AND DISCUSSION

In this section, first the tensile test results are reported. Following that, the fracture surfaces are examined by scanning electron microscopy.

Tensile Strength

The stress–strain curves of the ARBed samples have been obtained by a tensile test (Fig. 2). This figure shows that the tensile strength increases by the number of cycles greatly. This change between cycle#0 and cycle#1 is very considerable. In all the ARBed samples, the flow stress reaches its maximum value rapidly. This means that macroscopic necking occurs in a lower elongation. The strength of the primary composite reaches its maximum value (187 Mpa) after cycle#0.

Figure 3 indicates the variation of the ultimate tensile strength of the samples versus the rolling cycles. By repeating the process, the strength of the samples increases continuously to five cycles (with a maximum value of 362 Mpa). The strengthening

Table I. The chemical compositions of AA1050 and AA5083

	Element	Al	Cr	Si	Fe	Mn	Zn	Ti	Cu	Mg
AA1050	wt.%	Balance	0.0016	0.12	0.222	0.032	0.01	0.005	0.12	–
AA5083	wt.%	Balance	0.21	0.23	0.185	0.51	0.23	0.003	0.08	4.5

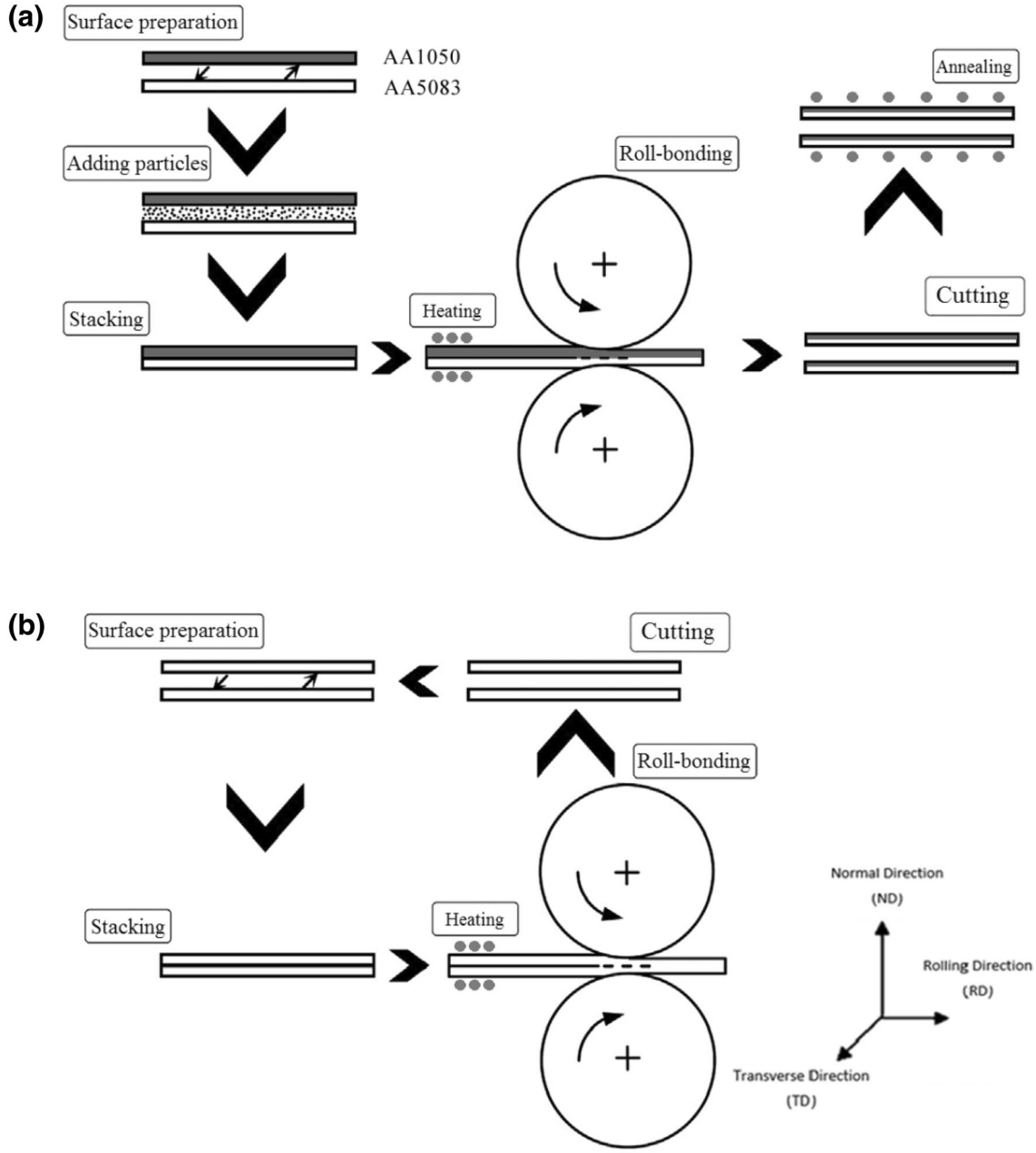

Fig. 1. Schematic illustration of the production process of the Al/Al_2O_3 composite sheet: (a) primary cycle (cycle#0) and (b) main cycles.

Table II. Specifications of the warm-ARB process for the production of the composite

No. of cycles	Rolling temperature (°C)	No. of Al-layers	No. of Al_2O_3 layers	Reduction in each cycle (%)	Total reduction (%)	Effective strain (ε_{ef})
0	400	2	1	75	75[a]	1.6[a]
1	280	4	2	50	50	0.8
2	280	8	4	50	75	1.6
3	280	16	8	50	87.5	2.4
4	280	32	16	50	93.75	3.2
5	280	64	32	50	96.87	4

[a]After cycle#0, the sample is annealed at 400°C for 1 h; therefore, the strain exerted in cycle#0 would be removed.

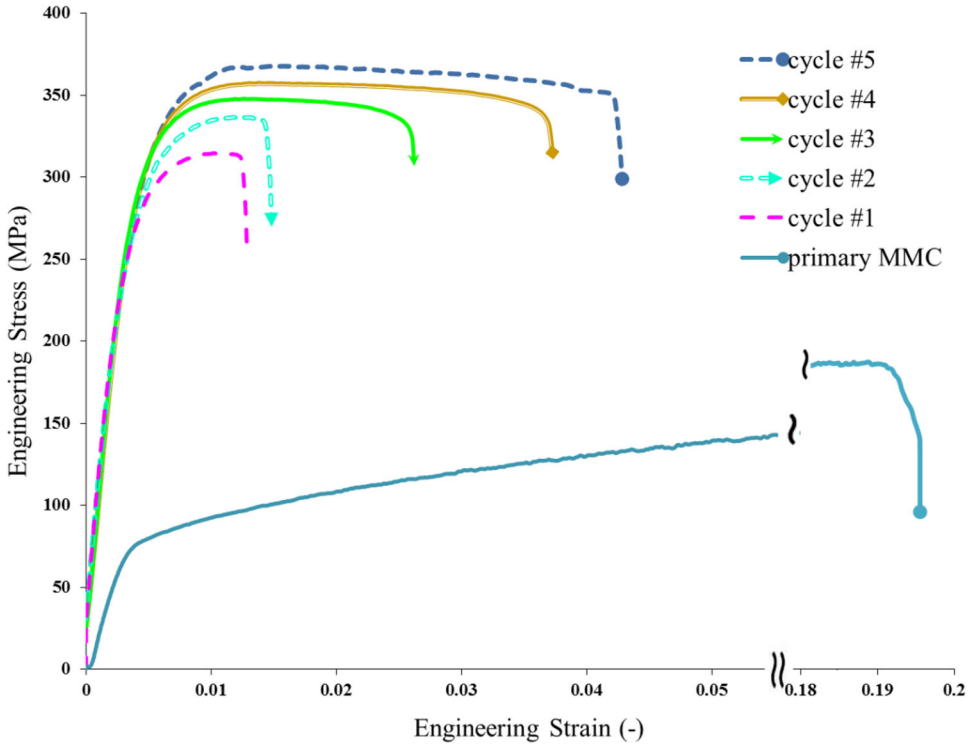

Fig. 2. Engineering stress–strain curves for AA1050/Al_2O_3/AA5083 composites before and after warm-ARB (average of three tests).

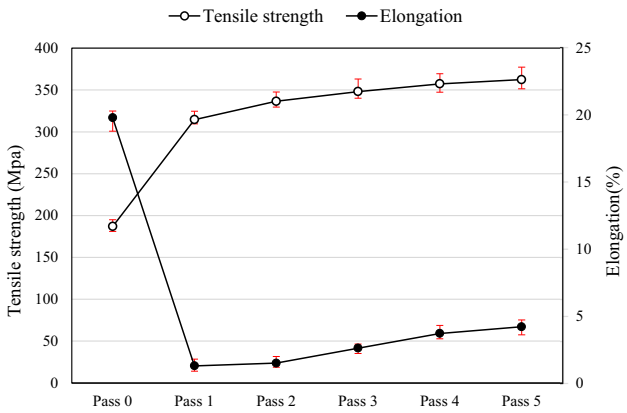

Fig. 3. Mechanical properties of the AA1050/Al_2O_3/AA5083 composites, produced by the warm-ARB process in various cycles.

behavior could be based on two mechanisms which are due to dislocation strengthening and grain boundary strengthening.[26]

According to Fig. 3, after the first cycle, the elongation of the samples decreases severely, and their elongation subsequently begins to improve from cycle#1 to cycle#5. This behavior is attributed to (1) increasing the uniformity of the particles, (2) increasing the bond strength between the Al alloy matrixes, and (3) decreasing the porosities in the clusters. By increasing the number of ARB cycles, the bond between the layers improves with a good continuity. Furthermore, the metal matrix flows among the clusters, leading to the increase in the distance between the alumina particles.[27]

As the hardening rate of AA5083 is significantly higher than that of AA1050, the strength of the AA5083 layers in the composite exceeds that of the AA1050 layers. Accordingly, the AA5083 layers are strain-hardened faster than the AA1050 layers. In the first three ARB cycles, the thinning of the AA5083 layers occurs in the same way as the AA1050 layers. At higher numbers of cycles, the deformation becomes inhomogeneous, and the thickness of the AA5083 layers starts to change along the rolling direction. After cycle#3, the AA5083 layers begin necking in some regions with further deformation (Fig. 4b and c). Then, the adjacent AA1050 layer in higher numbers of cycles follows the necking process (Fig. 5).

Figure 6 demonstrates the variations of toughness with various ARB cycles. The toughness value of the composites declines considerably from cycle#0 (19.51×10^4 j m^{-3}) up to cycle#1 (3.4×10^4 j m^{-3}). This behavior is due to the work hardening and less movement of the dislocations.[27] The toughness value of the composites increases gradually during the ARB process up to cycle#2 (4.2 j $m^{-3} \times 10^4$). However, this change has a faster pace up to cycle#5 (14.61×10^4 j m^{-3}). Enhancing the strength and the strain amplitudes of the samples during the ARB process leads to higher toughness of the fabricated 1050/5% Al_2O_3/5083 composites (Fig. 6).

Three types of the combination of the samples were prepared (1050–1050, 1050–5083, and 5083–5083) which contain alumina powder as reinforcement particles between each two layers. A

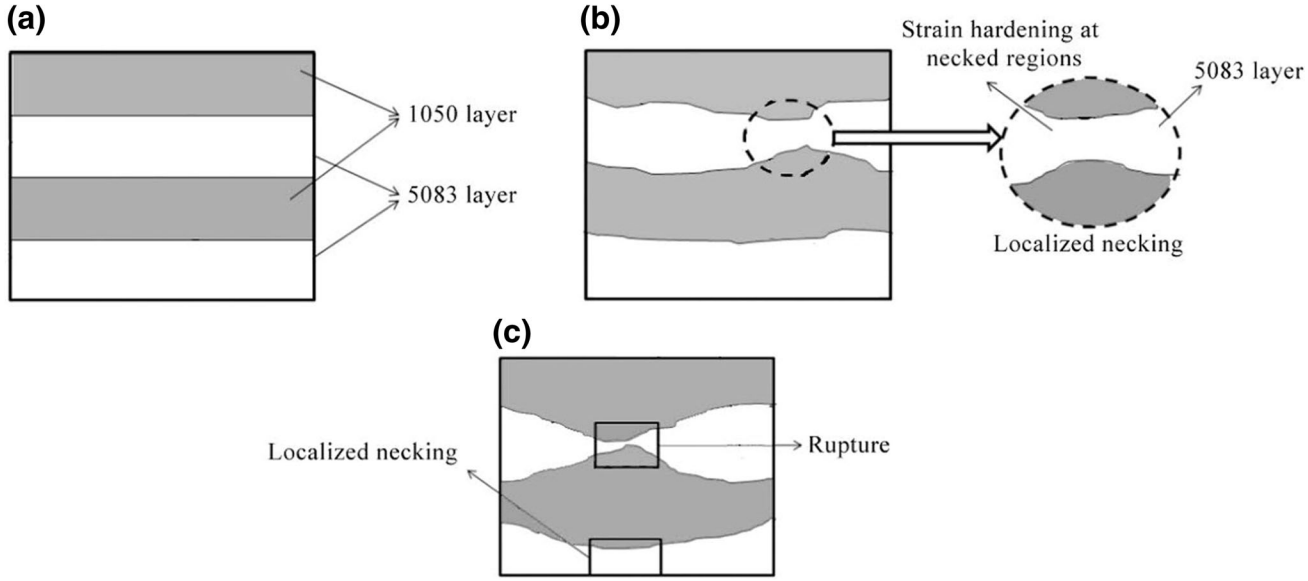

Fig. 4. SEM micrographs of specimens after Warm-ARB processing for (a) primary cycle (cycle#0), (b) three cycles and (c) five cycles.

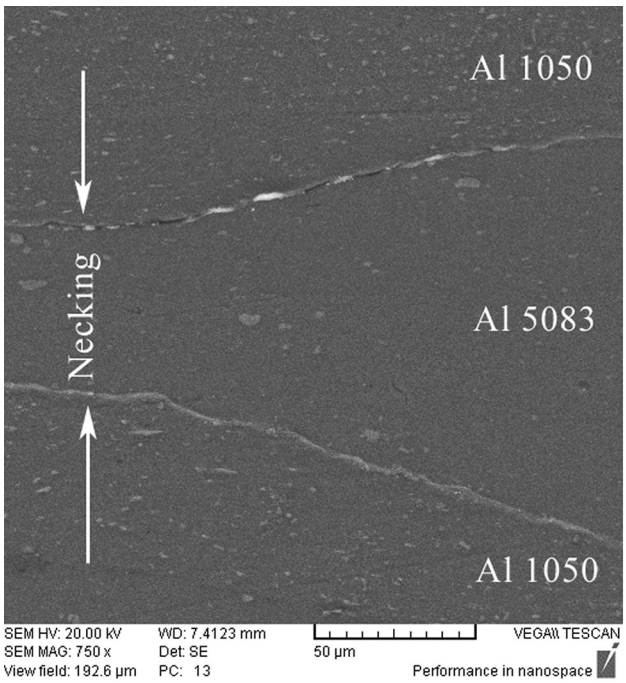

Fig. 5. SEM micrographs of warm-ARB processed materials after five cycles.

comparison between the ultimate tensile strength of the MMCS and the numbers of ARB cycles is presented in Fig. 7. The UTS of all samples grows at higher numbers of cycles. The strength of the 1050–5083 samples in each cycle is between the amplitudes of the 1050–1050 and 5083–5083 samples and is higher than their average amplitudes.

The elongation of all the three types of samples diminishes substantially after 1 cycle of the ARB process and remains almost unchanged with further

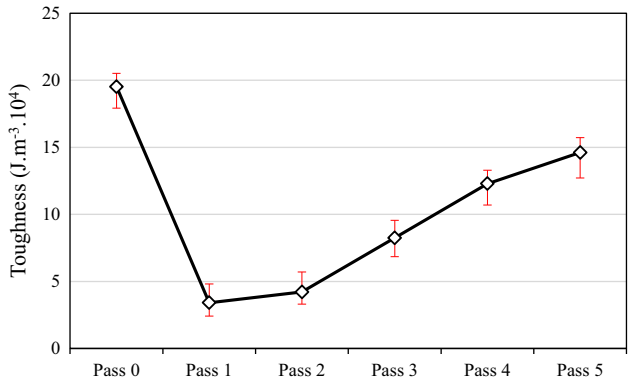

Fig. 6. Variations of toughness with the warm-ARB cycles.

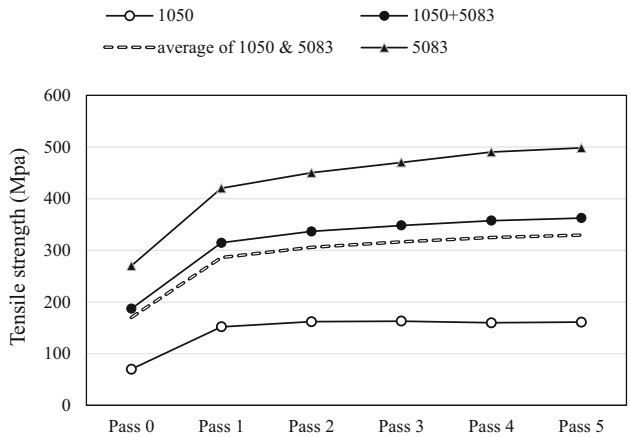

Fig. 7. Mechanical properties of samples produced by various ARB cycles.

plastic deformation (Fig. 8). The elongations of all three types of materials are $<7\%$. By increasing the ARB cycles, the elongation of all samples increases.

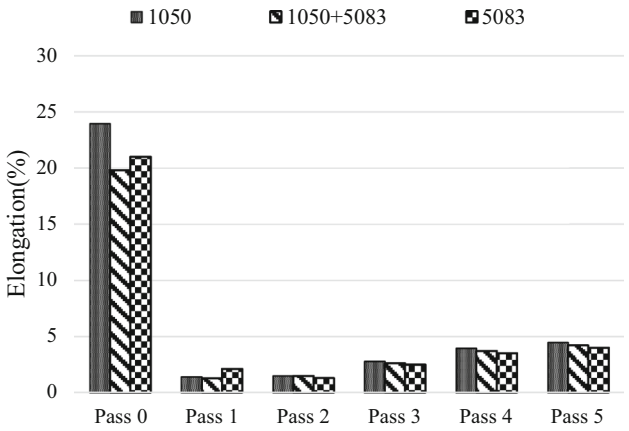

Fig. 8. Variations of maximum elongation of samples by various ARB cycles.

The elongation amplitude of the 1050–5083 samples in each cycle is between the amplitudes of the 1050–1050 and 5083–5083 samples.

Fractography

A scanning electron microscopic (SEM) study was applied in order to investigate the rupture mechanism in the primary sandwich and the products after 1, 2, 3, 4, and 5 ARB cycles. The fracture surfaces after the tensile test of the composites are presented in Figs. 9 and 10. The zone of AA1050 in cycle#1 exhibits a typical ductile fracture and deep dimples (Fig. 9a and b). In addition, the zone of AA5083 in the same cycle demonstrates a fracture surface with shear zones and shallow dimples (Fig. 9c and d). This difference illustrates that the rate of work hardening in AA5083 is more than that of AA1050. Figure 10b–d clearly reveals that the composites with three, four, and five cycles exhibit a fracture surface with dimples and shear zones. By increasing the number of ARB cycles, the fracture

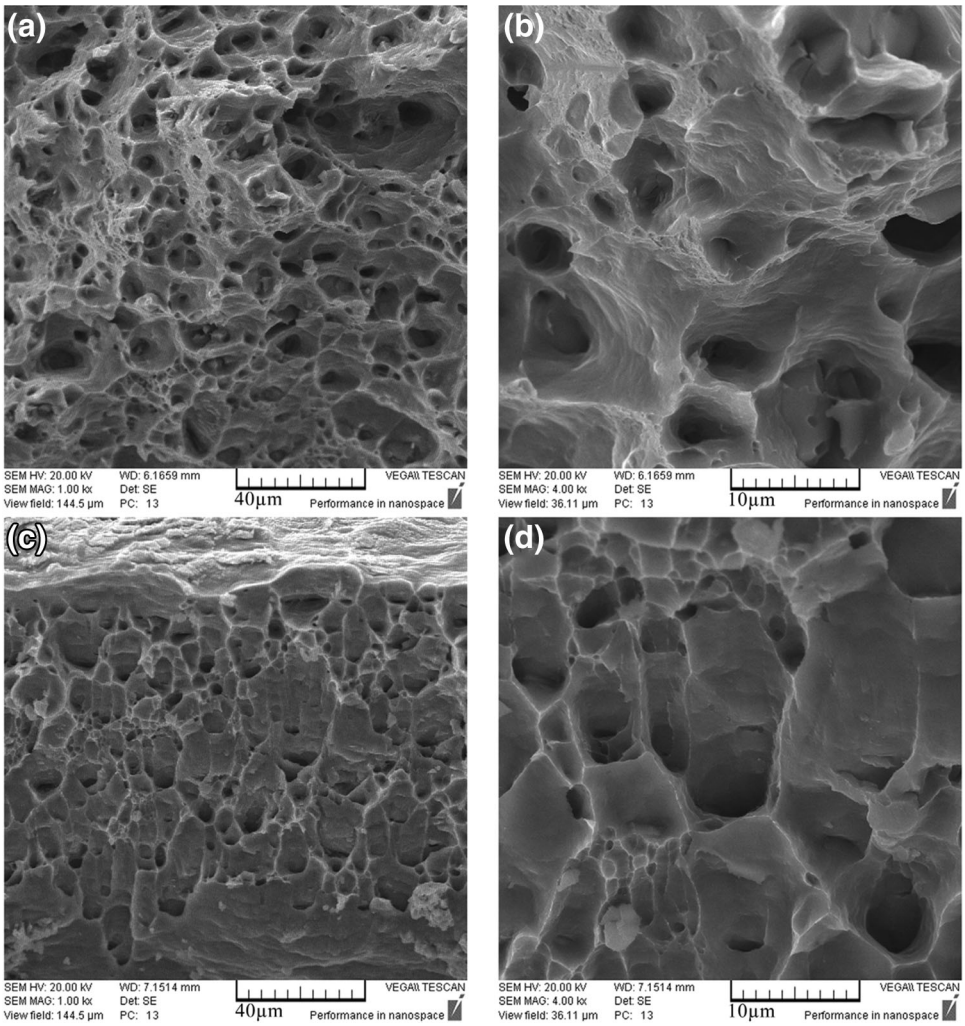

Fig. 9. The fracture surfaces after tensile test for: (a, b) zone of AA1050 and (c, d) zone of AA5083 in composite with one cycle of warm-ARB. They are shown in two magnifications.

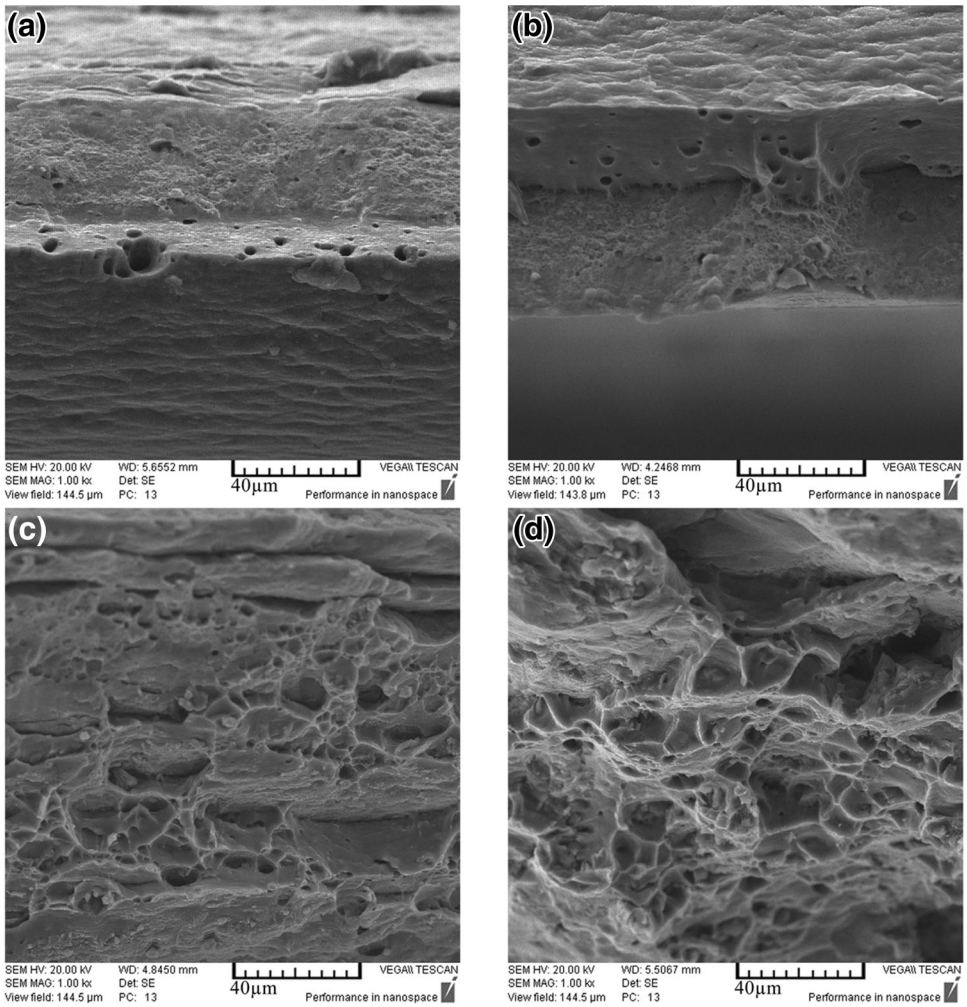

Fig. 10. The fracture surfaces after tensile test for cycles: (a) 2, (b) 3, (c) 4 and (d) 5 with warm-ARB cycles after tensile testing.

surface is not as deep as the prior cycles, and the deep dimples are slowly shrinking. Furthermore, the main fracture surfaces do not have dimples with an elongated and deep shape. The nucleation of the micro-voids, their growth in the structure, and finally their coalescence, which is affected by shear stress, generate these dimples.[28] The presence of alumina particles on the core and walls of the dimples implies that these particles provided suitable sites for crack initiation and nucleation. As weak places in the structure, particle–matrix interfaces are appropriate places for crack propagation.[29] Finally, at lower numbers of cycles, the fracture surfaces have deep and elongated dimples, while at cycle#5, the dimples are not deep and elongated as a result of the work-hardened matrix.

CONCLUSION

In this paper, a warm-ARB method was proposed to combine two different aluminum alloys for obtaining Al-based MMCs containing 5% alumina particles. Regarding the behavior of this combination, the following findings can be highlighted:

1. The tensile strength of the composites increases along with the ARB cycles and reaches a maximum value of 362 MPa at cycle#5, which is about 2 times higher than the strength of the primary sandwich.
2. The maximum elongation of primary sandwich (annealed) is 20% which reduces sharply to 1.3% after the first cycle. However, it increases to 4.2% at the cycle#5.
3. The toughness of primary sandwich is 19.5×10^4 j m^{-3}, while the toughness after the first cycle is 3.4×10^4 j m^{-3} which is less than that of the primary composite. By increasing the number of cycles, the toughness reaches 14.6×10^4 j m^{-3} at cycle#5. In other words, the alumina particles enhance the toughness of the composites at higher ARB cycles.
4. During the first three ARB-cycles, both the AA1050 and AA5083 layers deform in a nearly identical way. But afterwards, the necking of AA5083 layers leads to the dispersion of these harder fragments into the AA1050 matrix, increasing the strength of the final MMC with

respect to the average amplitude of the AA1050–AA1050 and AA5083–AA5083 MMC samples.

REFERENCES

1. J.C. Williams and E.A. Starke, *Acta Mater.* 51, 5775 (2003).
2. H. Demir and S. Gündüz, *Mater. Des.* 30, 1480 (2009).
3. C.W. Schmidt, C. Knieke, V. Maier, H.W. Höppel, W. Peukert, and M. Göken, *Scr. Mater.* 64, 245 (2011).
4. L. Vaidyanath, M. Nicholas, and D. Milner, *Br. Weld. J.* 6, 13 (1959).
5. S.V. Prasad and R. Asthana, *Tribol. Lett.* 17, 445 (2004).
6. Y. Saito, H. Utsunomiya, N. Tsuji, and T. Sakai, *Acta Mater.* 47, 579 (1999).
7. Y. Saito, N. Tsuji, H. Utsunomiya, T. Sakai, and R.G. Hong, *Scr. Mater.* 39, 1221 (1998).
8. M. Paramsothy, N. Srikanth, and M. Gupta, *J. Alloys Compd.* 461, 200 (2008).
9. M. Paramsothy, S.F. Hassan, N. Srikanth, and M. Gupta, *J. Alloys Compd.* 482, 73 (2009).
10. M. Paramsothy, N. Srikanth, S.F. Hassan, and M. Gupta, *Mater. Sci. Eng. A* 494, 436 (2008).
11. M. Paramsothy, S.F. Hassan, N. Srikanth, and M. Gupta, *J. Phys. D Appl. Phys.* 41, 175402 (2008).
12. H.S. Liu, B. Zhang, and G.P. Zhang, *Scr. Mater.* 64, 13 (2011).
13. A. Mozaffari, H. Danesh Manesh, and K. Janghorban, *J. Alloys Compd.* 489, 103 (2010).
14. R.N. Dehsorkhi, F. Qods, and M. Tajally, *Mater. Sci. Eng. A* 530, 63 (2011).
15. L. Ghalandari and M.M. Moshksar, *J. Alloys Compd.* 506, 172 (2010).
16. M.Z. Quadir, O. Al-Buhamad, L. Bassman, and M. Ferry, *Acta Mater.* 55, 5438 (2007).
17. T. Hausöl, H.W. Höppel, and M. Göken, *J. Mater. Sci.* 45, 4733 (2010).
18. S. Roy, B.R. Nataraj, S. Suwas, S. Kumar, and K. Chattopadhyay, *Mater. Des.* 36, 529 (2012).
19. L. Su, C. Lu, A.K. Tieu, G. Deng, and X. Sun, *Mater. Sci. Eng. A* 559, 345 (2013).
20. V.K. Lindroos and M.J. Talvitie, *J. Mater. Process. Technol.* 53, 273 (1995).
21. C. Liu, Q. Wang, Y. Jia, B. Zhang, and R. Jing, *Mater. Des.* 43, 367 (2013).
22. C. Lu, K. Tieu, and D. Wexler, *J. Mater. Process. Technol.* 209, 4830 (2009).
23. M. Eizadjou and H. Danesh, Manesh, and K. Janghorban. *Mater. Des.* 29, 909 (2008).
24. J.E. Hatch, *Properties Aluminium, and Physical Metallurgy*, Vol. 143 (Metals Park: American Society for Metals, 1984).
25. ASTM, in *Annu. B. ASTM Stand.*, Vol. 4 (ASTM International, 2010), p. 1.
26. M. Alizadeh, M.H. Paydar, and F. Sharifian Jazi, *Compos. Part B Eng.* 44, 339 (2013).
27. M. Rezayat, A. Akbarzadeh, and A. Owhadi, *Compos. Part A Appl. Sci. Manuf.* 43, 261 (2012).
28. M. Eizadjou, H.D. Manesh, and K. Janghorban, *J. Alloys Compd.* 474, 406 (2009).
29. R. Jamaati and M.R. Toroghinejad, *Mater. Sci. Eng. A* 527, 7430 (2010).